Journal of Materials Chemistry A

Accepted Manuscript

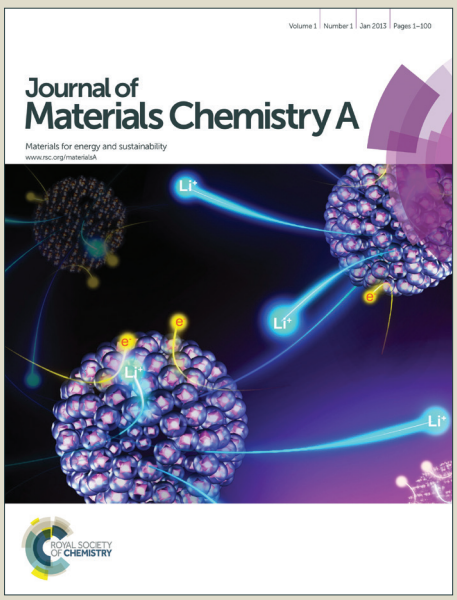

ROYAL SOCIETY OF CHEMISTRY

www.rsc.org/materialsA

Cite this: DOI: 10.1039/x0xx00000x

A nanotubular framework with customized conductivity and porosity for efficient oxidation and reduction of water

Jun Wu,[a, b] Lianwen Zhu,[*,b] Dan Deng,[c] Longfeng Zhu,[b] Li Gu[c] and Xuebo Cao[*,b]

Received 00th January 2012,
Accepted 00th January 2012

DOI: 10.1039/x0xx00000x

www.rsc.org/

To reduce the total cost of production of hydrogen and oxygen from water splitting, many efforts have been made to develop first row transition metal materials instead of precious platinum–group catalysts. Recently, porous catalysts with high conductivity for hydrogen evolution reaction (HER) and oxygen evolution reaction (OER) have attracted more attention. Here, a quaternary inorganic framework consisting of Ni^0 and $Ni(OH)_2$, graphite–like C, and titanate nanotubes (referred to as Ni^x/C/TNTs framework) has been successfully fabricated. Compared to the precious Pt/C for HER and IrO_2/C OER, the fabricated Ni^x/C/TNTs framework exhibited highly activities towards the water splitting. At a current density of 10 mA/cm^2, its OER overpotential is as small as 280 mV while its HER overpotential is as small as 145 mV. The excellent electrochemical performance can be attributed to its unique structure of Ni^x/C/TNTs framework that can effectively expand the interface, maximize the reacting sites, and thus guarantee rapid mass and electron transfer.

Introduction

To reduce the total cost of production of hydrogen and oxygen from water splitting, many efforts have been made to develop first row transition metal materials instead of precious platinum–group catalysts.[1-9] At present, the critical issue of notorious overpotentials from the current non-precious catalysts for the H_2– and O_2–evolution half reactions (HER and OER) is still not addressed. It is mainly due to the use of non precious catalyst that deteriorate water–splitting kinetics and decrease the energy efficiency.[10] For example, commercial Ni electrode exhibits a large OER overpotential of 519 mV and HER overpotential of 747 mV at the current density of 10 mA/cm^2.[11]

For electrochemical reactions taking with an appreciable current, the overpotential η can be expressed by an empirical formula named Tafel equation $\eta = a + blogj$,[12] where a and b are the constants associated with surface states and electrochemical characteristics of the catalyst while j is the current density. Tafel equation clearly suggests that the maximization of electrochemically active surface area (EASA) of a given OER/HER catalyst will be a straightforward solution to the notorious overpotential because it is able to minimize the current density j. Besides the large EASA, long–range electronic connectivity is also strongly demanded by OER/HER catalysts.[13, 14] This is because electrochemical water splitting involves electron transfer reactions at the interface and electron transport in the electrode.[15] Therefore, some three–dimensional (3D) conducting matrixes, such as Ni foam[16, 17] and nanoporous carbon materials,[18-20] were recently developed to load first row of transition metal materials for the purpose of achieving the desirable conductivity and porosity.

Inorganic frameworks featured by the porosity tuneable from molecular to macroscopic level have long been considered to be the optimal geometry for OER/HER catalysts.[21] It is because the micro– and mesoporosity is able to expand the surface area and shorten diffusion paths of electrolytes while the meso– and macroporosity favour the access of catalytically active sites and the escape of evolved gases. The extensive porosity, however, is often in conflict with the long–range electronic connectivity,[22] because the conductivity relies on the structural coherence while the porosity is in proportion to grain boundaries. Therefore, substantial progress in the design and synthesis of extensively porous OER/HER catalysts is still remained a challenge, especially when the customized electronic connectivity is expected simultaneously.

Here we report that a quaternary inorganic framework consisting of Ni^0 and $Ni(OH)_2$ species, graphite–like C, and titanate nanotubes (referred to as Ni^x/C/TNTs framework) can meet both criteria and deliver activities towards the two half reactions of water splitting. Each of the quaternary components specifically contributes to the performance of the framework as an overall water–splitting electrode: (1) the TNTs spontaneously organize into a giant framework to endow the system with five levels of interconnected pores; (2) Ni^0 and $Ni(OH)_2$ crystallites offer the binary active sites for HER and OER, respectively; (3) the graphite–like C behaves as "conducting cement" to transform Ni^x/C/TNTs framework into an efficient electron percolation network and bridge the framework and the underlying Ni foam backbone. As a consequence, the nanotubular Ni^x/C/TNTs framework demonstrates HER performances comparable to the precious Pt/C (20 wt% Pt on Vulcan XC–72) and OER performances comparable to the precious IrO_2/C (20 wt% IrO_2 on Vulcan XC–72) in the electrolyte of 0.1 M KOH.

Experimental Section

Synthesis of Ni^x/C/TNTs Framework. All chemicals were analytical grade, purchased from Shanghai Chemical Reagents Company, and used without further purification. Prior to the synthesis of Ni^x/C/TNTs framework, the Ni foam was treated by 0.1 M HCl solution containing polyvinylpyrrolidone (PVP) at 80 °C for 30 mins to enhance the hydrophilicity of the surface.

The synthesis of Ni^x/C/TNTs framework comprises four primary steps. Firstly, a piece of Ni foam with arbitrary size and shape was repeatedly dipped in the solution dispersed by TiO_2 nanoparticles (average particle size ~ 80 nm) and SiO_2 microspheres (diameter ~300 nm) in a weight ratio of 2:1. Due

to the capillary effect, TiO_2 and SiO_2 migrated into the voids within the Ni foam. Secondly, the modified Ni foam was impregnated in furfurylalcohol (FFA) added by *p*–toluenesulfonic acid (0.1 mmol of *p*–toluenesulfonic acid per 1 g of FFA). Thirdly, the Ni foam was heated at a rate of 2 °C min^{-1} to 120 °C under flowing nitrogen, held at 120 °C for 2 h, then heated to 200 °C at 2°C min^{-1} and held at 200 °C for 2 h, and finally heated to 800 °C at 2°C min^{-1} and held at 800 °C for 4 h. The sample was found to change the colour from the initial white to black, indicative of the conversion of FFA to carbon. Finally, the Ni foam was placed into a Teflon–lined stainless steel autoclave containing 10 M NaOH solution and the sealed autoclave was heated at 140 °C for 36 h. After completing the hydrothermal reaction, the Ni foam was taken out from the autoclave and washed to neutral with de-ionized water. Thus, Ni^x/C/TNTs framework anchored on the Ni foam was prepared. For comparison, the control samples of C–coated Ni foam and single TNTs framework anchored on the Ni foam were also prepared by employing the similar procedures described above. In addition, we also prepared the reference Ni^x/C/TNTs framework in the absence of the 300-nm SiO_2 microspheres.

Characterizations of Morphology and Structure of Ni^x/C/TNTs Framework. Scanning electron microscopy (SEM) measurement was performed on a Hitachi S–4800 field emission instrument, operating at an accelerating voltage of 10 kV. Transmission electron microscopy (TEM) measurement was performed using a FEI Tecnai G2 instrument operating at 200 kV. To prepare TEM samples, Ni^x/C/TNTs framework was detached from Ni foam backbone by ultrasonic method, dispersed in ethanol, and deposited onto a carbon–coated copper grid. Powder X–ray diffraction (XRD) measurements were performed on a Bruker D8 X–ray diffractometer using Cu Kα radiation (λ = 0.15405 nm). XPS spectra were obtained with an ESCALAB MK II X–ray photoelectron spectrometer (XPS) using an Al Kα source. Samples for XRD and XPS measurements were the powders detached from the Ni foam backbone. Nitrogen adsorption–desorption isotherms and porosity were measured on a Micromeritics ASAP 2020 instrument. Elemental analysis were performed with Energy Dispersive X–ray (EDX) spectrometers attached on the HITACHI S–4800 or FEI Tecnai G2 electron microscope. Thermogravimetric (TG) analyses of the products were performed on a STA–409 PC thermal analyzer.

Electrical conductivity measurements. The electrical conductivities of Ni^x/C/TNTs framework were measured by a two–probe method. Firstly, Ni^x/C/TNTs was detached from the Ni foam and the collected powders were pressed into a pellet with a diameter of 13 mm and a thickness of 0.5 mm. Then, the pellet was sandwiched between two copper electrodes and connected to a CHI 660 potentiostat–galvanostat (CH Instruments Inc.) for conductivity measurements.

Alternating Current (AC) Impedance Measurements. Electrochemical impedance spectroscopy (EIS) data for Ni^x/C/TNTs framework were recorded with a Zahner Im6ex instrument under the following conditions: ac voltage amplitude 5 mV, frequency ranges 0.01 Hz to 100 kHz, and open circuit.

Electrochemically Active Surface Area (EASA) Measurements. EASA of the samples was determined by the potential step method.[23] Firstly, the working electrode was stabilized in 0.1 M KOH until the open circuit potential (OCP) became constant. Then, the chronoamperometric curve was recorded with a potential step of ($\Delta\varphi$ = 5 mV) and an impulse width of 15 s.

Evaluations of OER and HER Performances of Ni^x/C/TNTs Framework. OER and HER performances of Ni^x/C/TNTs were evaluated in a standard three–electrode glass cell, by directly using Ni^x/C/TNTs framework anchored on the Ni foam as a working electrode (size: 1 cm × 1 cm), a Pt plate as a counter electrode, Ag/AgCl/KCl (saturated) as a reference electrode, and CHI 660C to collect data. Electrolytes for HER and OER studies were 0.1 M KOH (pH ~13) and O_2–saturated 0.1 M KOH, respectively. OER polarization curves, HER polarization curves, and Tafel plots were obtained at a scan rate of 1 mV/s. The current density was normalized to the geometrical area and the measured potentials vs Ag/AgCl were converted to a reversible hydrogen electrode (RHE) scale according to the Nernst equation ($E_{RHE} = E_{Ag/AgCl} + pH \times 0.059 + 0.1976$ V). The overpotential η was calculated according to the following formula: η (V) = E_{RHE} –1.23 V. For comparisons, the HER and OER performances of bare Ni foam (1 cm × 1 cm), C-coated Ni foam, single TNTs framework, 20 wt% Pt/C, 20 wt% IrO_2/C, and the reference Ni^x/C/TNTs framework were studied under the conditions identical to those for Ni^x/C/TNTs framework. To prepare the Pt/C (or IrO_2/C) samples, 35 mg 20 wt% Pt/C (or IrO_2/C) was dispersed in 10 mL distilled water and 20 μl 5 wt% Nafion solution with 30 min sonication treatment to form a homogeneous ink. Then, this solution was deposited onto a 1 cm × 1 cm Ni foam.

Results and Discussion

Scheme 1a describes the synthesis strategy of Ni^x/C/TNTs framework. Since Ni foam has a large number of merits in the field of electrochemistry (e.g., porous structure, high electron conductivity, favourable electrocatalytic activity, low cost, etc.),[16, 17] it was selected as the support of Ni^x/C/TNTs frameworks. In the step 1, SiO_2 microspheres and TiO_2 nanoparticles were introduced into the voids of the Ni foam (ESI, Fig. S1a), which would serve as the sacrificial templates to form macropores and as the raw materials to synthesize TNTs,[24-26] respectively. In the step 2, SiO_2 microspheres and TiO_2 nanoparticles anchored on the Ni foam were impregnated in FFA, which had been reported to be a superior organic precursor for deriving conductive carbon.[27] The subsequent pyrolysis of FFA (Step 3) would lead to the formation of a thin layer of carbon coated on the surfaces of TiO_2, SiO_2, and Ni foam (Fig. S1b and S1c). The carbon coatings are expected to act as "conducting cements" in the final system. It will not only enable the insulating TNTs framework to transport electrons but also bridge the framework and the Ni foam backbone. In the final step, an alkaline hydrothermal process was applied to the Ni foam filled

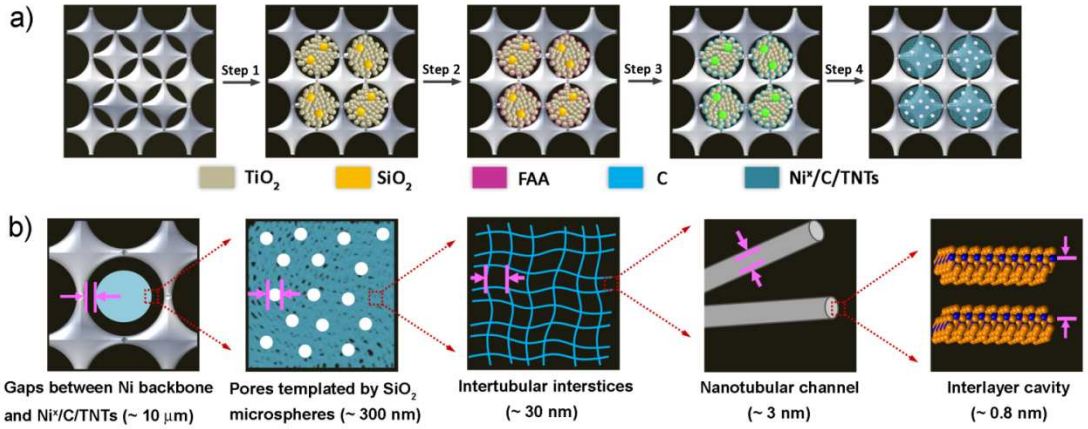

Scheme 1 (a) Schematic drawing illustrating the procedures to the preparation of Ni^x/C/TNTs supported by Ni foam (referred to as Ni^x/C/TNTs/Ni). (b) Cartoon of the multimodal porosity ranging from the micrometer to molecule level.

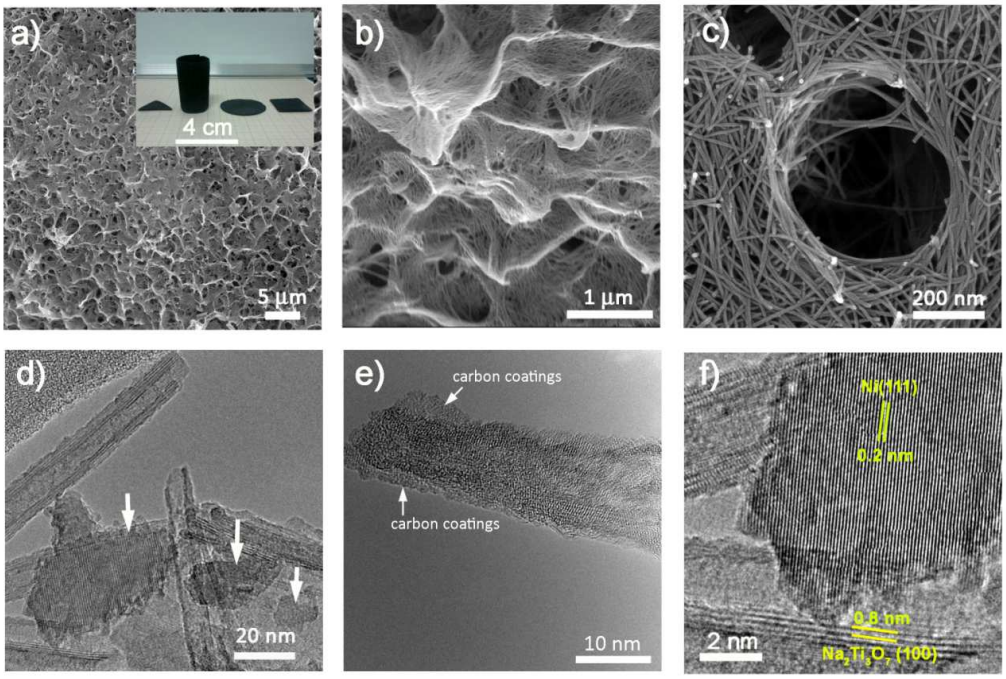

Fig. 1 (a) Top-view and (b) side-view SEM images of Ni^x/C/TNTs framework (inset: optical image showing Ni^x/C/TNTs grown on the Ni foam). **(**c) SEM image of Ni^x/C/TNTs with a high magnification. (d) TEM image of Ni^x/C/TNTs, where the arrows denote laminar Ni^0 species. (e) TEM image exhibiting the coating of C on the nanotube. (f) HRTEM image of the laminar crystallite and the nanotube.

by TiO_2 nanoparticles, SiO_2 microspheres and the pyrogenic carbon. Such a treatment could etch SiO_2 to generate sub–micron grade of holes, convert TiO_2 into interconnected titanate nanotube framework, and yield Ni^0 and Ni^{2+} species by using the Ni foam as the source. Thus, Ni^x/C/TNTs framework integrating the desirable multi–scale porosity, long–range conductivity, and binary catalytic sites for both water oxidation and reduction reactions was readily prepared. Through the calculation of the increase in mass of the Ni

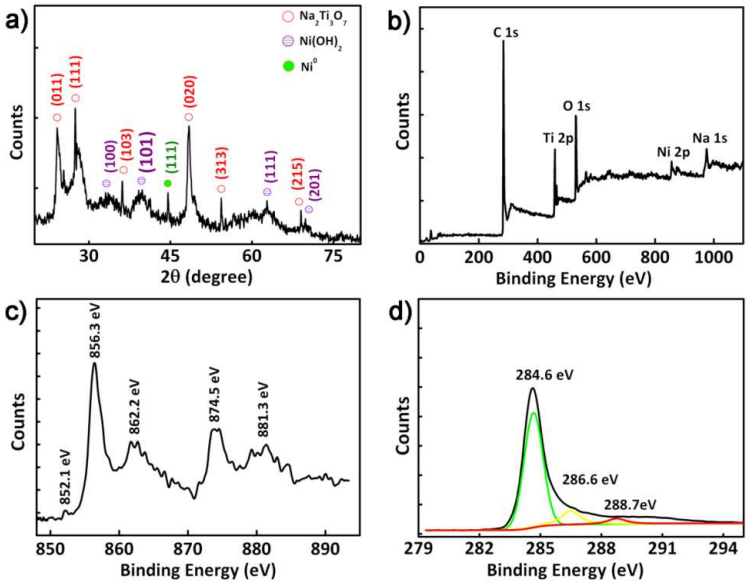

Fig. 2 (a) XRD pattern of Ni^x/C/TNTs framework. (b) XPS survey spectrum of Ni^x/C/TNTs framework. (c) Ni 2p binding energy spectrum. (d) C 1s binding energy spectrum.

foam, the mass loading of Ni^x/C/TNTs framework was determined as 35 mg/cm^2.

The as–prepared Ni^x/C/TNTs framework anchored on the Ni foam is shown in the inset of Fig. 1a. The optical image demonstrates that the shape and size of Ni^x/C/TNTs framework can be optionally manipulated according to the specific demands, which is beneficial from the flexibility of the substrate of the Ni foam. Fig. 1a–c display the SEM characterizations of Ni^x/C/TNTs frameworks. From the top–view (Fig. 1a) and side–view (Fig. 1b) SEM images, it is seen that the framework is constructed by interpenetrated nanotubes. A high–magnification SEM image (Fig. 1c) reveals that there not only exist abundant nanoscale interstices among the neighboring nanotubes but also sub–micron grade of holes templated by sacrificial SiO_2 (~300 nm; statistical density ~ 4 × 10^9 holes/cm^2). To determine the average width of the interstice, nitrogen adsorption–desorption characterizations of the Ni^x/C/TNTs frameworks were performed. The large hysteresis in the P/P_0 range of 0.4~1.0 indicates the mesoporosity of the sample (Fig. S2a). From the BJH pore–size distribution plots calculated from the desorption branch (Fig. S2b), two kinds of mesopores (pore widths: ~ 37 nm and ~ 2.8 nm) are distinguishable: the former is attributed to the nanoscale interstices among the neighboring nanotubes and the latter corresponds to the inner diameter of the nanotubes. Additionally, micrometer level of gaps (~10 μm) are observed between Ni^x/C/TNTs framework and the backbone of Ni foam (Fig. S3); their widths far exceed the sizes of the above–mentioned macropores and mesopores.

Fig. 1d shows the TEM characterization of Ni^x/C/TNTs framework, which reveals that the nanotubes have a multiwalled structure and open terminations (interwall distance ~0.8 nm; inner diameter ~ 3 nm). Each wall of the nanotubes represents a (100) plane of titanate rolled around the *b*–axis,[24] between which are positioned by exchangeable Na^+ ions.[24, 28] In short, both SEM and TEM data indicate that the proposed strategy (Scheme 1a) is able to develop a total of five levels of pores with pore width spanning over the scale of micrometer, sub–micron, nanometer, and angstrom (Scheme 1b). In particular, the multimodal pores are interconnected in space, thereby effectively expanding the interface, maximizing the reacting sites, and guaranteeing rapid mass transfer and gas escape.[21]

Fig. 1e shows the HRTEM image of an individual nanotube. Different from the clean surfaces of pristine TNTs (Fig. S4),[25] there is a sharp contrast between the inside nanotube and the outside sheath for the nanotube herein, which indicates the coating of a layer of carbon. Moreover, well–crystalline laminar crystallites laid flat on the nanotubes are frequently observed during the TEM measurements, such as the ones marked by arrows (Fig. 1d). They are assigned to zerovalent nickel species (Ni^0) on the basis of the resolved interplanar distance (~ 0.2 nm, matching well with the neighboring (111) lattices of elemental nickel). In addition to the laminar Ni^0 crystallites, irregular fine crystallites belonging to the hexagonal $Ni(OH)_2$ are also observed in the sample (Fig. S5).

To further verify the coexistence of zerovalent and bivalent Ni species in the Ni^x/C/TNTs framework, the powdered samples detached from the support of Ni foam were investigated by the techniques of XRD and XPS. Fig. 2a shows the XRD pattern of the sample, where the diffraction peaks belonging to Ni^0, $Ni(OH)_2$, and sodium titanate were all detected, confirming the multi–component constitution of the framework. Fig. 2b shows the XPS survey spectrum of the sample. No impurities are detected except for the

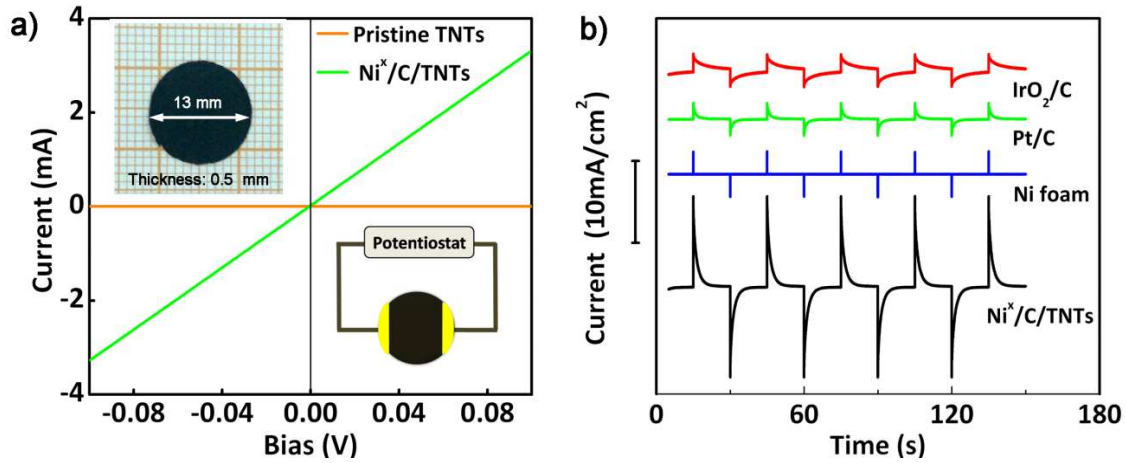

Fig. 3 Ni^x/C/TNTs framework exhibiting long-range electronic connectivity and large EASA. (a) room temperature *I–V* curves of Ni^x/C/TNTs framework and pristine TNTs. Inset: the pellet pressed by Ni^x/C/TNTs framework powders and the two–probe method for conductivity measurements. (b) *I* vs. *t* profiles for potential–step measurements of Ni^x/C/TNTs framework, bare Ni foam, Pt/C, and IrO_2/C.

elements associated with Ni^x/C/TNTs framework (C, O, Ni, Ti, and Na). According to the element–sensitive mapping analysis (Fig. S6), the elements of C, O, Ni, Ti, and Na are homogeneously distributed in the framework. Fig. 2c shows Ni2p core–level binding energy spectrum, where the peak at 852.1 eV is typical for Ni^0 species while the Ni2p lines at 856.3 eV and 874.5 eV with shoulders on the higher binding energy sides correspond to Ni–O species in $Ni(OH)_2$.[29, 30] As seen, the results of XPS are consistent with the above–mentioned XRD and electron microscopy data. "Volcano plot" has demonstrated that Ni^0 is the viable alternative to Pt group HER catalysts,[31] and $Ni(OH)_2$/NiOOH phases are active for OER.[21, 32] Consequently, the binary valence states of Ni species in Ni^x/C/TNTs framework may lead to the novel catalyst with overall activities for water splitting.

Fig. 2d shows the C1s core–level spectrum. The asymmetric profile can be fitted to a dominant peak around 284.6 eV (graphitic C) and two insignificant peaks around 286.6 eV (hydroxyl C) and 288.7 eV (carboxyl C), which implies the high graphitization of C and the residue of oxygen–containing groups. With the crosslinking of the highly graphitized C, Ni^x/C/TNTs framework may become an effective electron percolation network capable of prompt charge transfer. Simultaneously, the residual oxygen–containing groups are also helpful, as they render Ni^x/C/TNTs framework somewhat hydrophilic and facilitate the interactions with water molecules to expedite the catalytic process.[20]

To elucidate the development of the Ni^0 and $Ni(OH)_2$ crystallites in the Ni^x/C/TNTs framework, we monitored the intermediates by the techniques of XRD and SEM. XRD data (Fig. S7) demonstrate that the phases of Ni^0 and $Ni(OH)_2$ were detected at the stage of the pyrolysis of FFA (Step 3, Scheme 1a) and the stage of alkaline hydrothermal treatment (Step 4, scheme 1a), respectively. SEM measurements show that, after the pyrolysis of FFA, the backbone of the Ni foam was cleaved (Fig. S8), which is the consequence of the corrosion of the Ni foam caused by various organic matters under the high temperature conditions (e.g., the infiltrated FFA and *p*–toluenesulfonic acid and their pyrolysis intermediates). The results demonstrate that the introduction of Ni^0 into the framework is ascribed to the exfoliation of laminar nickel crystallites from the Ni foam. The generation of $Ni(OH)_2$ crystallites is also ascribed to the corrosion of the Ni foam, which occurred in the alkaline hydrothermal environment.[33] As seen, with the proposed strategy, both Ni^0 and Ni^{2+} species can be introduced into the framework by utilizing the Ni foam as the source, which are the potential HER and OER active sites, respectively.

The powdered Ni^x/C/TNTs framework was then pressed into a pellet for conductance measurements (Fig. 3a). Different from the electrical insulation of pristine TNTs,[24, 34] the Ni^x/C/TNTs framework exhibits a large electronic conductivity (~ 280 S/m), which is sufficient for many electrochemical applications.[35] Moreover, alternating–current impedance spectroscopy characterizations demonstrate that Ni^x/C/TNTs framework also exhibits a small charge–transfer impedance (~ 3.7 Ω) in the electrolyte of 0.1 M KOH (Fig. S9). The remarkably small size of the semicircle in the high–frequency region (< 0.2 Ω) suggests the favorable ion transport within the highly developed pores of the framework.[36] Next, the EASA of Ni^x/C/TNTs framework anchored on the 1 cm^2 Ni foam was determined by the potential–step method in the electrolyte of 0.1 M KOH (Fig. 3b).[23] For comparison, we also studied the EASA of Pt/C, IrO_2/C and bare Ni foam under identical conditions. The double layer capacity (C_d) and the EASA of the samples were calculated by the following equations:

$$C_d = \frac{\Delta Q}{\Delta \varphi} = \frac{\int_0^\infty i dt}{\Delta \varphi} \qquad \text{(Eq. 1)}$$

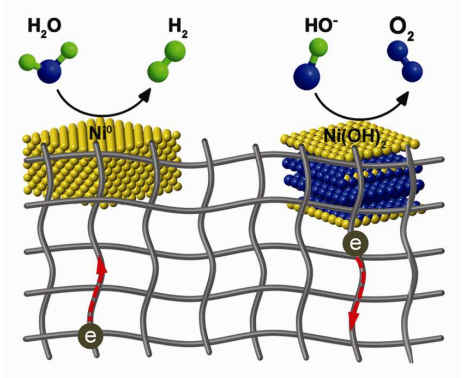

Scheme 2 Illustration of the bifunctionality of Ni^x/C/TNTs framework in both HER and OER.

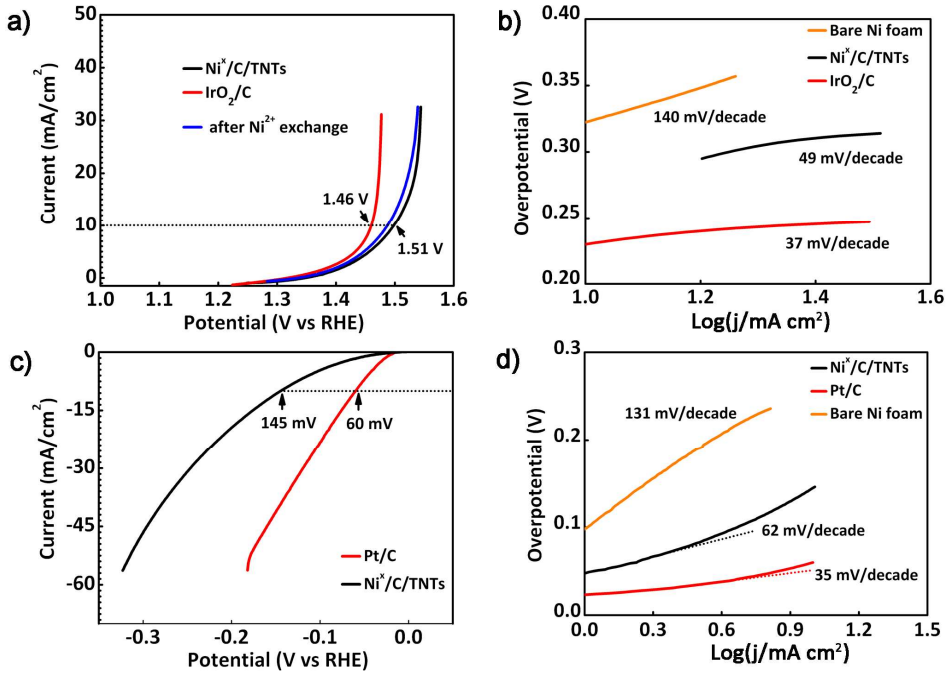

Fig. 4 Overall activities of Ni^x/C/TNTs framework for electrochemical water splitting. (a) OER polarization curves of Ni^x/C/TNTs framework in comparison to IrO_2/C and (b) corresponding Tafel plots (electrolyte: O_2-saturated 0.1 M KOH; Scanning rate: 1 mV/s). (c) HER polarization curves of Ni^x/C/TNTs framework in comparison to Pt/C and (d) corresponding Tafel plots (electrolyte: 0.1 M KOH; Scanning rate: 1 mV/s).

$$EASA = \frac{C_d}{C_{Hg}} \qquad \text{(Eq. 2)}$$

C_{Hg} in Eq. 2 is the capacitance of pure mercury (20 μF cm^{-2}), which is a commonly used reference parameter for determining the effective area. Relative to these samples, a much larger peak area is distinguished in the chronoamperometric curve of Ni^x/C/TNTs framework, indicative of the remarkable difference in the accessible surface of these samples. By calculating the double layer capacitances (C_d) and comparing them with the capacitance of pure mercury (20 μF cm^{-2}),[23] the EASA of Ni^x/C/TNTs framework anchored on the 1 cm^2 Ni foam was estimated to be 39000 cm^2. In contrast, the EASA for Pt/C and IrO_2/C anchored on 1 cm^2 Ni foam (loading level: 35 mg/cm^2) and bare 1 cm^2 Ni foam are 6100 cm^2, 8200 cm^2, and 156 cm^2, respectively. These results confirm the effectiveness of the extensive pores in expanding the interface of Ni^x/C/TNTs framework. With the remarkable EASA, the actual current density *j* flowing through Ni^x/C/TNTs framework will be significantly reduced and *blogj* in the Tafel equation will be negligible, so that OER/HER overpotentials will not deteriorate even at large current densities.

Beneficial from the combination of large EASA, long–range electronic connectivity, and binary Ni^x species, Ni^x/C/TNTs framework should promise well–performed activities in both OER and HER (Scheme 2). Firstly, we evaluate its OER performance in 0.1 M KOH saturated by O_2, by directly adopting the framework anchored on the Ni foam as the working electrode. From the polarization curve (Fig. 4a), it is seen that the anodic currents began to rise after the applied potential is larger than 1.30 V vs reversible hydrogen electrode (RHE; all potentials reported here are with respect to this reference). When the applied potential exceeds 1.55 V, the anodic current increases steeply. Since the O_2/H_2O equilibrium potential is 1.23 V vs RHE, 1.30 V corresponds to only 70 mV of overpotential for water oxidation, which outperforms

other Ni–based OER catalysts reported.[16, 17, 20] Further stability tests demonstrate that Ni^x/C/TNTs framework retains the activity well after 800 potential cycles (Fig. S10). After the cycle tests, the sample was characterized again by the techniques of SEM, XRD and chronoamperometry (Fig. S11). Fig. S11a shows the SEM image, which revealed that the sample still maintained the hierarchically porous structure. Figure 1b shows the chronoamperometric data, which reveals that the EASA for the sample after the cycle is decreased by 4.9%. The decrease of EASA is understandable because the porous sample may absorb certain substances from the electrolyte after the long operation. XRD pattern of the sample is also basically identical to the original one except the weakening of the peak assigned to Ni^0. The weakened Ni^0 peak suggests the retarded oxidation of the Ni nanoplates during the long-term OER operation.

In contrast, the control samples, such as the bulk Ni foam, C–coated Ni foam (Fig. S12a), and single TNTs framework anchored on the Ni foam (Fig. S12b), all exhibited poor OER performances (Fig. S13). The comparison demonstrates the indispensability of each component in Ni^x/C/TNTs framework. In addition, notable anodic waves (~ 1.38 V) ascribed to the oxidization of the Ni foam backbone are developed in control experiments (Fig. S13),[17] while it is absent for Ni^x/C/TNTs framework. The superior corrosion resistance of Ni^x/C/TNTs framework is attributed to the passivation of Ni^0 species under alkaline hydrothermal conditions[37] and the formation of protective C around the backbone of the Ni foam (Fig. S14).[16] We also compared our Ni^x/C/TNTs framework with commercial IrO_2/C anchored on the Ni foam, since IrO_2 is identified as the most active OER catalyst in both acid and base.[13, 38] The loading level of IrO_2/C is 35 mg/cm^2, same as that for Ni^x/C/TNTs framework. As shown in Fig. 4a, Ni^x/C/TNTs framework can afford a current density of 10 mA/cm^2 at the potential close to that of IrO_2/C (1.51 V vs 1.46 V). Further, the Tafel slope, an important kinetic parameter, is measured to be 49 mV/decade for Ni^x/C/TNTs framework, approaching that of IrO_2/C (Fig. 4b). These results demonstrate that, after the impartment of extensive porosity and excellent conductivity, Ni^x/C/TNTs framework can compare favorably with the state of the art OER catalysts.[11] Moreover, by taking advantaging of the exchangeability of Na^+ located inside the walls of TNTs,[24, 28] more $Ni(OH)_2$ crystallites can be introduced into Ni^x/C/TNTs framework to yield more OER active centers (Fig. S15). In response, the OER current density can be increased by 32.7% at the potential of 1.5 V (Fig. 4a).

After the verification of the OER performance of Ni^x/C/TNTs framework in 0.1 M KOH, we switched the potential to the regime of water reduction to evaluate its HER performance. When the potential is negative than -50 mV, HER current was yielded on the Ni^x/C/TNTs framework electrode (Fig. 4c), which suggests a small potential onset. Further, Ni^x/C/TNTs framework affords large current densities at low overpotentials (e.g., 10 mA/cm^2 at -145 mV) and a small Tafel slope of 67 mV/decade (Fig. 4d). These performances approach commercial Pt/C (Fig. 4c and 4d), while far surpass the control samples (Fig. S16), such as the bare Ni foam, C–coated Ni foam (Fig. S12a), and single TNTs framework anchored on the Ni foam (Fig. S12b). Moreover, Ni^x/C/TNTs framework is also a durable HER catalyst, as the stability tests demonstrate a little current attenuation after the 10000 mins of operation (Fig. S17). These results make Ni^x/C/TNTs framework a powerful catalyst with overall activities for water splitting.

Theoretically, both the Ni^0 species embedded in the framework and the Ni foam backbone underlying the framework are the possible active sites for HER. However, since the Ni backbone was surrounded by the dense carbon spheres (Fig. S14), the plate-like Ni^0 species are more accessible by the electrolyte, and hence, should play a dominant role in the HER. In addition, two different phenomena may also suggest that the Ni^0 nanoplates are the major active sites for HER. One is the oxidation resistance of the Ni backbones in the OER experiments, indicative of the difficulty for the access of the electrolyte. It is necessary to note that, although the Ni^0 nanoplates is accessible by the electrolyte, no remarkable anodic wave from its oxidation was observed. It is because the content of the Ni^0 nanoplates is low in the framework and its oxidation current is negligible when compared to that from OER. The other phenomenon is that no black particles were peeled off from the Ni foam after the long-term HER operation. If HER were occurred at the sites of the Ni backbone, the Ni^x/C/TNTs framework would be peeled off from the Ni backbone by hydrogen bubbles.[39]

Besides the control samples of the bare Ni foam, C–coated Ni foam, and the single TNTs framework anchored on the Ni foam, we also studied the OER and HER performances of the Ni^x/C/TNTs framework without the 300 nm of pores (Fig. S18). The reference Ni^x/C/TNTs framework was prepared without using the SiO_2 microspheres as the sacrificial templates (other conditions were kept identical to those for preparing the normal Ni^x/C/TNTs framework). Compared to the Ni^x/C/TNTs framework with the 300 nm of pores, the Ni^x/C/TNTs framework without the 300 nm of pores yield a relatively low OER and HER current density (Fig. S13 and S16). However, it still outperforms the samples of the bare Ni foam, C–coated Ni foam, and the single titanate nanotube framework supported by the Ni foam. Fig. S19 and S20 show the Tafel plots for OER and HER on the Ni^x/C/TNTs framework with and without the 300 nm of pores, both of which reveal that the porous ones has a lower Tafel slope (49 mV/decade vs 109 mV/decade for OER and 62 mV/decade vs 83 mV/decade for HER). The above results further highlight the importance of the porous structure and the synergistic effect among the quaternary components.

Motivated by the bifunctionality and effectiveness of Ni^x/C/TNTs framework, we proceeded to investigate its practical utility and therefore fabricated a two–compartment alkaline water electrolyser (Fig. S21). In the device, Ni^x/C/TNTs frameworks replaced conventional noble metals as the anode and the cathode. At an operating voltage of 1.6 V (370 mV larger than theoretical decomposition voltage of water), abundant bubbles formed on both the cathodic and the anodic Ni^x/C/TNTs framework, indicative of simultaneous production of H_2 and O_2 ($2H_2O + 2e \rightarrow H_2 + 2OH^-$; $4OH^- \rightarrow 2H_2O + O_2 + 4e$) at the low overpotential. Furthermore, hydrogen bubbles were sustained without slowing over the course of one hour electrolysis, manifesting the reliability of the material and its great potential for real–world application.

Conclusions

In conclusion, based on the understanding of electrochemically active area and conductivity in improving the performances of electrocatalysts, we engineer a nanotube–based inorganic framework from earth–abundant materials. With the synergetic effects among the quaternary components (titanate nanotubes, graphite-like C, Ni^0 crystallites, and $Ni(OH)_2$ crystallites), the framework is capable of integrating multimodal pores, long–range electronic connectivity, and in situ generated binary active sites for catalyzing the oxidation half reaction and the reduction half reaction of water splitting. As a consequence, the framework exhibits HER performances comparable to Pt/C and OER performances comparable to IrO_2/C. These results should lead to improved strategies for

the future investigations on the fabrication of effective water splitting electrocatalysts with advanced structures. Further, since titanate has the potential for topotactic transformation into photoelectrochemically active TiO_2, the derived $Ni^x/C/TiO_2$ framework is anticipated to enable the development of more efficient and more economical water–splitting devices, which may utilize electricity and solar light as the combined driving forces.

Acknowledgements
This work is financially supported by the NSFC (21473079, 21107032) and the Department of Education of Zhejiang Province (Y201330088, Y201330035) .

Notes and references

[a] College of Chemistry, Chemical Engineering and Material Science, Soochow University, Suzhou, Jiangsu 215123, China
[b] School of Biology and Chemical Engineering, Jiaxing University, Jiaxing, Zhejiang 314001, China. E-mail: xbcao@mail.zjxu.edu.cn; lwzhu@mail.zjxu.edu.cn
[c] School of Materials and Textile Engineering, Jiaxing University, Jiaxing, Zhejiang, 314001, China

† Electronic Supplementary Information (ESI) available: XRD and SEM characterizations of the intermediates and the carbon layer, EDS mapping results of Ni^x/C/TNTs framework, Nitrogen adsorption–desorption isotherms and pore size distribution of Ni^x/C/TNTs framework, stability tests of Ni^x/C/TNTs framework, polarization curves of the control samples. See DOI: 10.1039/b000000x/

1 M. W. Kanan and D. G. Nocera, *Science* 2008, **321**, 1072.
2 Y. Liang, Y. Li, H. Wang, J. Zhou, J. Wang, T. Regier and H. Dai, *Nat. Mater.* 2011, **10**, 780.
3 V. Artero, M. Chavarot-Kerlidou and M. Fontecave, *Angew. Chem. Int. Ed.* 2011, **50**, 7238.
4 R. Subbaraman, D. Tripkovic, K. C. Chang, D. Strmcnik, A. P. Paulikas, P. Hirunsit, M. Chan, J. Greeley, V. Stamenkovic and N. M. Markovic, *Nat. Mater.* 2012, **11**, 550
5 W. F. Chen, K. Sasaki, C. Ma, A. I. Frenkel, N. Marinkovic, J. T. Muckerman, Y. Zhu and R. R. Adzic, *Angew. Chem. Int. Ed.* 2012, **51**, 6131.
6 R. L. Doyle, I. J. Godwin, M. P. Brandon and M. E. Lyons, *Phys. Chem. Chem. Phys.* 2013, **15**, 13737.
7 J. F. Xie, H. Zhang, S. Li, R. X. Wang, X. Sun, M. Zhou, J. F. Zhou, X. W. Lou and Y. Xie, *Adv. Mater.* 2013, **25**, 5807.
8 Y. F. Xu, M. R. Gao, Y. R. Zheng, J. Jiang and S. H. Yu, *Angew. Chem. Int. Ed.* 2013, **52**, 8546.
9 X. Liu, Z. Chang, L. Luo, T. Xu, X. Lei, J. Liu and X. Sun, *Chem. Mater.* 2014, **26**, 18895.
10 J. Ran, J. Zhang, J. Yu, M. Jaroniec and S. Z. Qiao, *Chem. Soc. Rev.* 2014, **43**, 7787.
11 C. Hull, International critical tables of numerical data, physics, chemistry and technology. National Academies: 1929; Vol. 6.
12 A. J. Bard and L. R. Faulkner, *Electrochemical methods: fundamentals and applications*. Wiley New York: 1980; Vol. 2.
13 S. Trasatti and G. Lodi, *Electrodes of conductive metallic oxides*. Elsevier Amsterdam: 1981
14 D. Voiry, M. Salehi, R. Silva, T. Fujita, M. Chen, T. Asefa, V. B. Shenoy, G. Eda and M. Chhowalla, *Nano Lett.* 2013, **13**, 6222.
15 J. Rossmeisl, A. Logadottir and J. K. Nørskov, *Chem. Phys.* 2005, **319**, 178.
16 J. Wang, H. X. Zhong, Y. L. Qin and X. B. Zhang, *Angew. Chem. Int. Ed.* 2013, **52**, 5248.
17 W. Zhou, X. J. Wu, X. Cao, X. Huang, C. Tan, J. Tian, H. Liu, J. Wang and H. Zhang, *Energy Environ. Sci.* 2013, **6**, 2921.
18 M. Jahan, Z. Liu and K. P. Loh, *Adv. Funct. Mater.* 2013, **23**, 5363.
19 D. Kong, H. Wang, Z. Lu and Y. Cui, *J. Am. Chem. Soc.* 2014, **136**, 4897.
20 S. Chen and S. Z. Qiao, *ACS Nano* 2013, **7**, 10190.
21 L. Trotochaud and S. W. Boettcher, *Scripta Mater.* 2014, **74**, 25.
22 E. J. W. Crossland, N. Noel, V. Sivaram, T. Leijtens, J. A. Alexander-Webber and H. J. Snaith, *Nature* 2013, **495**, 215.
23 Y. H. Liu, *Techniques for electrochemical measurement.* Beijing Institute of Aeronautics Press 1987.
24 D. V. Bavykin, J. M. Friedrich and F. C. Walsh, *Adv. Mater.* 2006, **18**, 2807.
25 P. Chen, L. Gu, X. Xue, M. Li and X. Cao, *Chem. Commun.* 2010, **46**, 5906.
26 X. Xue, L. Gu, X. Cao, Y. Song, L. Zhu and P. Chen, *J. Solid State Chem.* 2009, **182**, 2912.
27 B. Fang, J. H. Kim, M. Kim and J. S. Yu, *Chem. Mater.* 2009, **21**, 789.
28 V. D. A. Cardoso, A. G. D. Souza, P. P. Sartoratto and L. M. Nunes, *Colloids Surf. A* 2004, **248**, 145.
29 H. Nesbitt, D. Legrand and G. Bancroft, *Phys. Chem. Miner.* 2000, **27**, 357.
30 L. Trotochaud, J. K. Ranney, K. N. Williams and S. W. Boettcher, *J. Am. Chem. Soc.* 2012, **134**, 17253.
31 J. K. Nørskov, T. Bligaard, A. Logadottir, J. Kitchin, J. Chen, S. Pandelov and U. Stimming, *J. Electrochem. Soc.* 2005, **152**, J23.
32 M. Gao, W. Sheng, Z. Zhuang, Q. Fang, S. Gu, J. Jiang and Y. Yan, *J. Am. Chem. Soc.* 2014, **136**, 7077.
33 X. Cao, X. Xue, L. Zhu, P. Chen, Y. Song and M. Chen, *J. Mater. Chem.* 2010, **20**, 2322.
34 Y. Zhou, L. Zhu, L. Gu, S. Cao, L. Wang and X. Cao, *J. Mater. Chem.* 2012, **22** , 16890.
35 D. Chung, *J. Mater. Sci.* 2004, **39**, 2645.
36 L. Pan, G. Yu, D. Zhai, H. R. Lee, W. Zhao, N. Liu, H. Wang, B. C. K. Tee, Y. Shi and Y. Cui, *Proc. Natl. Acad. Sci. USA* 2012, **109**, 9287.
37 M. Yasuda, F. Takeya and F. Hine, *Corrosion* 1983, **39**, 399.
38 J. Kiwi and M. Grätzel, *Angew. Chem. Int. Ed. Engl.* 1978, **17**, 860.
39 L. Zhang, K. Xiong, S. G. Chen, L. Li, Z. H. Deng, Z.D. Wei, *J. Power Sour.* 2015, **274**, 114.

A nanotubular framework with customized conductivity and porosity for efficient oxidation and reduction of water

Jun Wu, Lianwen Zhu, Dan Deng, Longfeng Zhu, Li Gu and Xuebo Cao

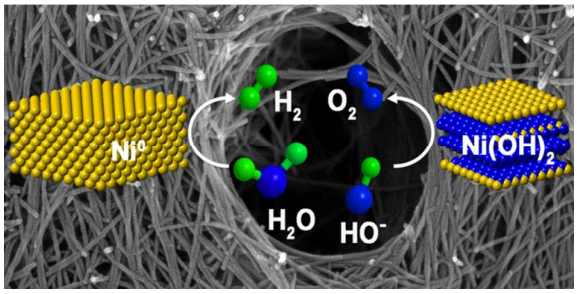

A quaternary inorganic nanotube framework delivering the efficient electrocatalytic activities towards the two half reactions of water splitting was designed.